Astron. Astrophys. 315, L55–L59 (1996)

ASTRONOMY AND ASTROPHYSICS

The photometric calibration of the ISO Short Wavelength Spectrometer*

S.G. Schaeidt[1,2], P.W. Morris[1,3], A. Salama[1], B. Vandenbussche[1,4], D.A. Beintema[1,5], D.R. Boxhoorn[1,5], H. Feuchtgruber[1,2], A.M. Heras[1], F. Lahuis[1,5], K. Leech[1], P.R. Roelfsema[1,5], E.A. Valentijn[1,5], O.H. Bauer[2], N.S. van der Bliek[7], M. Cohen[10], Th. de Graauw[5,8], L.N. Haser[2], K.A. van der Hucht[3], E. Huygen[4], R.O. Katterloher[2], M.F. Kessler[1], J. Koornneef[5] W. Luinge[5], D. Lutz[2], M. Planck[2], H. Spoon[2,3], C. Waelkens[4], L.B.F.M. Waters[6], E. Wieprecht[2], K.J. Wildeman[5] E. Young[9], and P. Zaal[6]

[1] ISO Science Operations Centre, Astrophysics Division of ESA, Postbox 50727, E-28080 Villafranca/Madrid, Spain
[2] Max-Planck-Institut für extraterrestrische Physik, Giessenbachstr. 1, D-85748 Garching, Germany
[3] SRON, Sorbonnelaan 2, 3584 CA Utrecht, The Netherlands
[4] Instituut voor Sterrenkunde, University of Leuven, Celestijnenlaan 200B, B-3001 Heverlee Belgium
[5] SRON, P.O. Box 800, 9700 AV Groningen, The Netherlands
[6] Astronomical Institute Anton Pannekoek, University of Amsterdam, Kruislaan 403, 1098SJ Amsterdam, The Netherlands
[7] Sterrewacht Leiden, Postbus 9513, 2300RA Leiden, The Netherlands
[8] Kapteyn Astronomical Institute, P.O. Box 800, 9700 AV Groningen, The Netherlands
[9] Steward Observatory, University of Arizona, Tucson, AZ 85721, USA
[10] Radio Astronomy Laboratory, University of California, Berkeley, California, CA 94720, USA

Received 1 August 1996 / Accepted 13 September 1996

Abstract. We give an overview of the photometric calibration of the Short Wavelength Spectrometer (SWS) through the Performance Verification phase. The basic strategy for deriving absolute flux densities from detector output for the grating and Fabry-Perot sections of SWS is reviewed, and the results are demonstrated with 2.4 – 45 μm spectra of representative standards γ Dra, α Lyr, and γ Cru. The effects of in-orbit changes in the relative spectral response function (RSRF) and ISO pointing are discussed. The systematic continuum flux level uncertainties (1 σ) are within the pre-launch specification of 30%. Further improvements depend on characterization of the in-orbit RSRF, improved performance of ISO pointing, and new data processing techniques.

Key words: instrumentation: spectrographs – methods: data analysis – infrared: general

1. Introduction

In this Letter we describe the preliminary, in-orbit photometric calibration of SWS. A description of the instrument, its observing modes, and data reduction methods is given by de Graauw et al. (1996). The wavelength calibration is described by Valentijn et al. (1996).

We begin with an overview of the calibration strategy, provide instrumental accuracy estimates, and summarize the primary SWS astronomical calibration sources (ACSs) on which the estimates are based. The impacts on the calibration by the in-orbit *vs.* pre-launch relative spectral response function (RSRF), and by ISO's pointing performance as measured by beam profiles are discussed. Finally, we point out certain instrumental and data handling issues which can contribute to the calibration error budget.

2. The Strategy of the Flux Calibration

In each of the 12 independent SWS grating and 5 independent SWS Fabry-Perot (F-P) AOT-bands (defined by detector block, aperture, and spectral order) we have chosen a wavelength and bandpass optimized to where the relative spectral response for each detector is at its maximum, and where the spectra of the ACSs are expected to be relatively featureless. So far unchanged, these so-called "key wavelengths" may be redefined where, for example, unexpected or particularly troublesome spectral features arise in the ACSs (e.g., SiO fundamental absorption in cool giants).

The SWS grating flux calibration is performed with a standard AOT6 grating scan of the ACS around each key wavelength within a specified bandpass (see Table 1). Flux calibration of the SWS F-P is performed with a special calibration uplink proce-

Send offprint requests to: P.W. Morris

* Based on observations made with the ISO, a project of ESA with the participation of ISAS and NASA, and the SWS, a joint project of SRON and MPE (DARA grants no 50 QI9402 3 and 50 QI 8610 8) with contributions from KU Leuven, Steward Observatory, and Phillips Laboratory.

Table 1. Summary of the flux calibration key wavelengths, bandpasses, and instrumental uncertainties by SWS AOT-band. Units for $\lambda_{\rm key}$ and $\Delta\lambda_{\rm key}$ are μm.

Band	1A	1B	1D	1E	2A	2B	2C	3A	3C	3D	3E	4	5A	5B	5C	5D	6
$\lambda_{\rm key}$	2.48	2.87	3.08	3.80	4.50	5.90	7.70	14.0	17.0	24.0	28.5	32.0	11.8	14.0	17.0	24.0	27.0
$\Delta\lambda_{\rm key}$	0.05	0.07	0.07	0.10	0.10	0.20	0.20	0.30	0.30	0.60	0.60	0.60	0.01	0.01	0.01	0.01	0.01
σ [%]	12	12	12	12	18	18	20	14	18	18	30	30	30	30	30	30	30

dure similar to the standard AOT7, but optimized in number of scans and step width for efficiency.

The fundamental photometric calibration of both grating and F-P sections can be summarized by the dependence of the absolute flux density $F(\lambda)$ of the observed source on various detector outputs and wavelength-dependent responsivities, taking into account time- and wavelength-dependent responsivity drifts:

$$F(\lambda) \;=\; S(\lambda)\frac{R(\lambda_{\rm key})}{R(\lambda)}\,\frac{S^d_{\rm ACS}}{S^d}\,\frac{F_{\rm ACS}(\lambda_{\rm key},\Delta\lambda_{\rm key})}{S_{\rm ACS}(\lambda_{\rm key},\Delta\lambda_{\rm key})} \qquad (1)$$

where

- $S(\lambda)$ is the detector output (in μV/s) at wavelength λ,
- $\lambda_{\rm key}$, $\Delta\lambda_{\rm key}$ refer to key wavelengths and bandpasses,
- $R(\lambda_{\rm key})/R(\lambda)$ is the responsivity normalization,
- $S^d_{\rm ACS}/S^d$ corrects for the time variation of detector response to the diffuse calibrator between observations of the ACS and the source,
- $F_{\rm ACS}/S_{\rm ACS}$ gives the conversion between μV/s and Jy from observations of the ACS at $\lambda_{\rm key}$.

For each detector these quantities are measured and stored in calibration tables that are called upon for pipeline processing of every observation in accordance with Eq. (1).

Accurate subtraction of dark currents from each detector's output is critical, and is problematic for sources of less than a few Jy, particularly in Band 4 (29.0-45.2 μm). To alleviate this problem, the photometric calibration tables are derived from the brightest sources (e.g., HR6705 or HR5340), and checked for linearity against fainter standards (e.g., HR7310). The contents of each calibration table are incorporated into a downlink (CAL-G) master table. *In principle*, more than one master table may exist to account for logic and responsivity changes over the course of the mission.

Approximate instrumental flux uncertainties are listed by AOT-band in Table 1. These are determined from systematic comparisons between AOT-S01 continuum levels and available reference data for the ACSs, with measured or adopted reference SED uncertainties added in quadrature. Systematic and non-systematic contributors to the uncertainties will be discussed in Section 6.

3. The SWS Calibration Sources and Examples

SWS relies primarily on stellar sources for relative and absolute calibration, subject to the constraints of visibility to ISO, brightness, stability (i.e., non-variability), and a point-like nature. In addition, a reliable SED must be available for each source. Table 2 summarizes the ACSs most heavily relied upon for the photometric calibrations and beam profile measurements. We must rely on more than one ACS because of visibility constraints, the wide range of wavelengths covered by SWS, varied spectral characteristics of flux standards, and the need to monitor responsivities at various brightness levels. It is also essential to monitor sources for cross-calibration with the other ISO instruments.

Reference SEDs consist primarily of model atmospheres and composite observations fit to photometry of the ISO ground-based preparatory programme (GBPP; van der Bliek et al. 1992) and elsewhere. Absolutely calibrated composite observed spectra are described by Cohen et al. (1992a,1995,1996). Composites for three of our main flux calibrators (γ Dra, α Boo, γ Cru; see Table 2) are documented by these authors, and are traceable to published calibrated spectra of Sirius and Vega (Cohen et al. 1992b).

For the standards of spectral types G9-K5 III, detailed MARCS model atmospheres suitable for both flux calibration and in-orbit derivations of the RSRF were generated using the Uppsala model atmosphere code MARCS Gustafsson et al. 1975, updated versions). Synthetic spectra for these model atmospheres were generated with the Synthetic Spectrum Generator code and line lists described by Bell & Gustafsson (1989); see also van der Bliek et al. (1996b). We also make use of LTE line-blanketed atmospheric models of Kurucz (1992) fit to stars of the GBPP by Dr. P. Hammerslay (priv. comm. to the ISO Calibration Working Group). Cohen et al. (1996) justify this procedure for the K and M giants.

The overall uncertainties on the SEDs are generally 4% - 10% of absolute levels, and are lowest at the shortest wavelengths; these are discussed by the authors (cf. van der Bliek et al. 1996a). The calibration of every source is ultimately tied to Vega observations, either to a V- or K-band magnitude whose adopted zero-point corrections result in baseline flux uncertainties of 2-3%.

Note that we do not include Solar System objects in Table 2. The asteroids Pallas and Ceres were initially chosen as calibrators for Bands 3 and 4 ($\lambda > 12$ μm) where high flux densities are predicted from the standard thermal model (T. Müller, priv. comm). However, these sources are not ideal for SWS due to errors caused by ISO tracking problems of fast-moving Solar System objects. This problem is most serious for calibration observations needed to derive the in-orbit RSRF.

NML Cyg presently replaces Pallas and Ceres in Bands 3 and 4 because of its brightness (exceeding 10^3 Jy) and good visibility. This is an enigmatic object, however, with suspected vari-

Table 2. Summary of primary SWS ACSs

Source	Alias	Spectral Type	Calib. Type[a]	Range [μm]
HR4763[b]	γ Cru	M4 III	f	12 – 35
HR5340[b]	α Boo	K1bCN III	FB	2.4 – 45.2
HR6705	γ Dra	K5 III	FR	2.4 – 28
HR7001[c]	α Lyr	A0 V	fR	2.4 – 16
HR7310	δ Dra	G9 III	fl	2.4 – 45.2
NML Cyg[d]	IRC+10448	M6 IIIe	fBR	16 – 45.2

Notes:
a: Calibration types – F = primary flux calibration source; f = secondary flux calibration source; l = linearity check; B = beam profile source; R = RSRF calibration source.
b: limited visibility.
c: Vega.
d: tertiary; see text.

ability, an HII region of unknown extent in the SWS apertures, and a high mass-loss rate. The tertiary nature of the available reference SED (low resolution and photometric uncertainty of 20% – 30%) warrants caution for using NML Cyg for responsivity measurements. In Band 4, we do use NML Cyg to check for *broad-band* discrepancies between the laboratory and in-orbit RSRF.

As examples of the flux calibration of grating scans from the key-wavelength observations of our primary standards, we show AOT1 scans of HR5340 and HR7001 (Fig. 1) flux-calibrated from mean responsivities (but weighted towards HR6705), and HR4763 (Fig. 2) whose calibration is based primarily on NML Cyg responsivities.

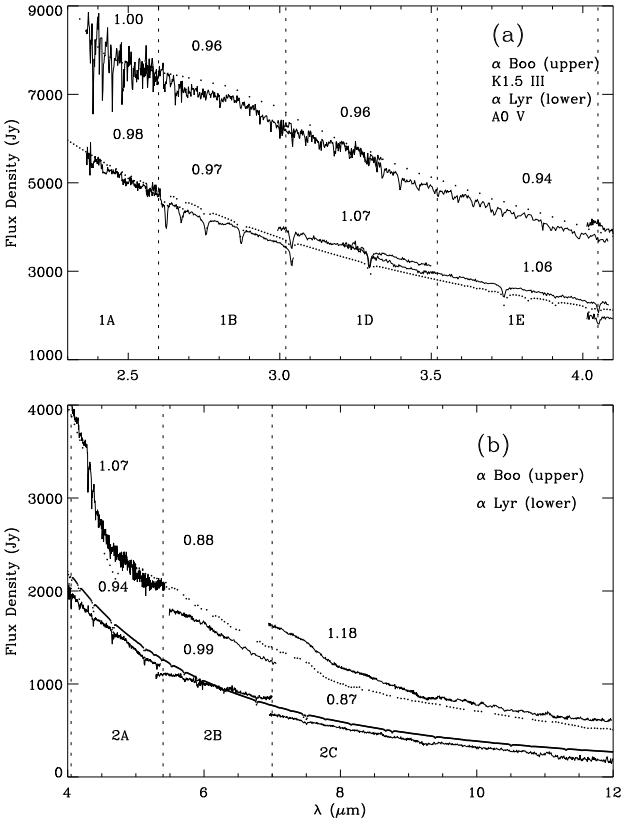

Fig. 1. AOT1 grating scans of α Boo and α Lyr (scaled by factor 10) in (a) Band 1 and (b) Band 2, compared with reference SEDs. Photometric calibration is based primarily on γ Dra. Dashed vertical lines indicate AOT-band limits. Numbers in each AOT-band refer to observed-to-reference flux ratios at the key wavelengths.

4. The SWS Relative Spectral Response Function

The relative spectral response of each detector to blackbody sources with a range of temperatures ($T_{\rm eff}$ = 30 – 300 K) filling the SWS aperture was measured prior to the launch of ISO during instrument level tests (ILT). Accuracy of the ILT responses was expected to be better than 30%, determined largely by the $\pm$1 K uncertainty of the blackbody temperature.

Since launch, the RSRF is being remeasured from special calibration observations of standard stars (see Table 1). The special mode of observation is more efficient than the standard grating scan mode and ensures additional wavelength overlap in each AOT-band at maximum grating resolution.

After the calibration observation is processed in the standard pipeline to the point of flux conversion, the RSRF for each detector is obtained by division with a reference SED. Extreme care is taken to inspect observations and SEDs for mismatches in the spectral features in order to avoid propagating these into the RSRF.

Two main differences between the ILT and in-orbit RSRF are summarized here:

1. Uncertainties of the overall shape are generally within the current uncertainties of the reference SEDs and the observations. Only at the short-wavelength edges of AOT-bands 1A and 2A have discrepancies warranted immediate correction, as the in-orbit relative responsivities are up to 60% lower. Figure 3 illustrates this difference for AOT-band 1A. Leakage in the ground-based measurements of the relatively cool blackbody source is believed responsible for this difference.
2. The detector-block filters of Bands 1 and 2 are now known to introduce fringes, whereas prior to launch only the large-amplitude fringes associated with resonances in the detectors of Band 3 were observed. The thickness of the filters in Bands 1 and 2 matches well with the F-P gap calculated from the observed fringe frequency. The width of the fringes is close to the resolution limit of the instrument, and thus the fringes could not be observed in the laboratory from the non-point like blackbody source.

Except for corrections applied to the broad-band shape of the relative spectral responsivities in AOT-bands 1A and 2A, all relative response corrections in the standard data processing currently utilize the ILT measurements. Uncertainty of the broad-band shapes of the remaining AOT-bands is probably no worse than $\sim$10%, by comparison to the ACSs, but verification is ongoing.

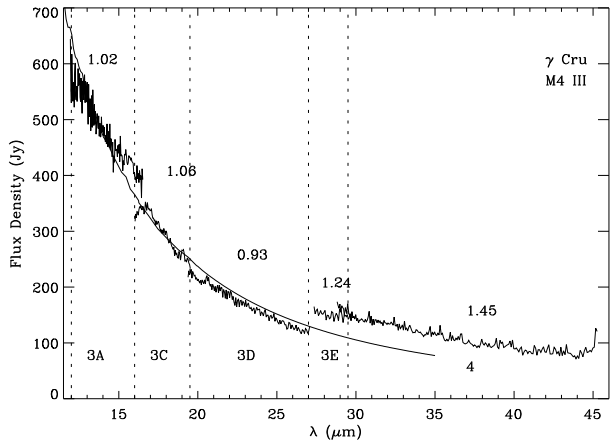

Fig. 2. AOT1 grating scan of γ Cru in Bands 3 and 4, compared to the reference SED. Here, photometric calibration is based on NML Cyg. Dashed lines indicate approximate AOT-band limits. Numbers in each AOT-band refer to observed-to-reference flux ratios at the key wavelengths.

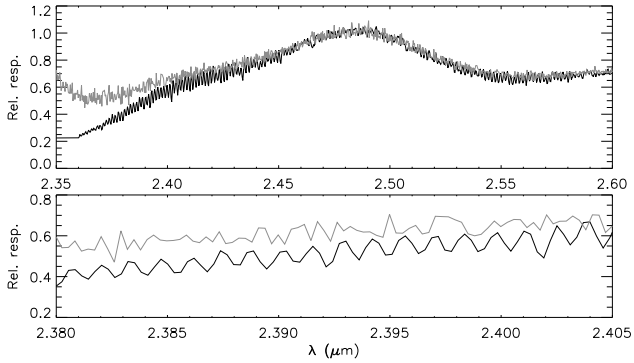

Fig. 3. The RSRF for AOT-band 1A derived from α Lyr observations (black) $vs.$ the RSRF as measured from an extended blackbody source in the laboratory (grey). The leakage is clearly visible in the laboratory measurement. As seen in the lower plot, only the in-orbit measurement (lower curve) fully resolves the fringes.

We are further verifying the *detailed* structure of the in-orbit RSRF, looking closely at fringe patterns and possible variations in spectral response over individual detector elements. Serious variations in response will introduce spectral features, but at present, *no* variations above the few percent level are immediately obvious. Derivation of detailed in-orbit RSRFs for Bands 1 and 2 is in progress. With future improvements in ISO's solar system tracking performance, we can derive the detailed relative responsivities for $\lambda > 12$ μm from Ceres, Uranus, and Saturn observations.

5. SWS Beam Profile Measurements and the Impact of ISO Pointing

The beam profiles have been measured by means of raster maps with oversampling factors of at least 3, around point-like sources (α Boo for the grating and NML Cyg for the F-P), in all AOT-bands. The scanners were held at fixed positions which correspond to the key wavelengths described above. The raster maps were designed to cover at least one diffraction beam outside the slit.

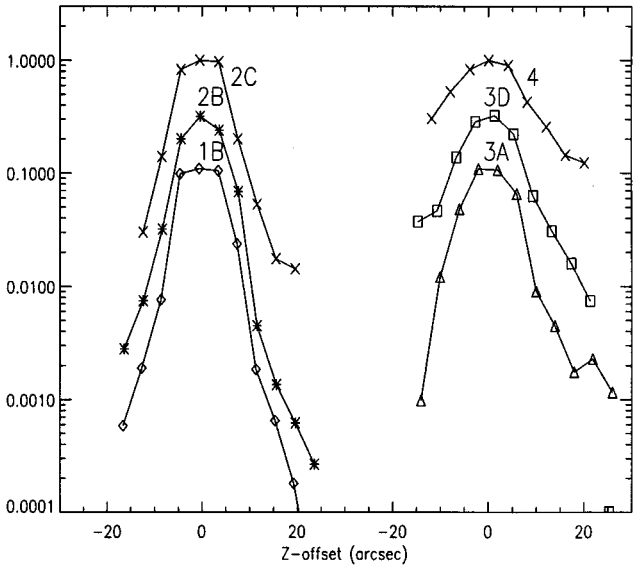

Fig. 4. Beam profiles for selected AOT-bands, normalized to the fitted peak response, and shifted by factors of 3 for clarity. For all AOT-bands indicated the slit width is $14''$, except Band 4, where it is $20''$.

In Figure 4 the resulting beam profiles are shown, normalized to the peak responses, where the median of detector responses for each detector array has been taken. For clarity, only the profiles in the dispersion direction are displayed by aperture for each of the two grating sections.

The absolute pointing accuracy of ISO was verified with the SWS at the start of a number of PV phase revolutions by means of quick cross-like maps, on the targets used for beam profile and on HR6705 and η Car. The peak-to-peak spread of all centroids is about $\pm 4''$. This translates via the beam profile curves into a contribution to the photometric error budget of at most 10% to 30%, depending on the AOT band. While ISO's pointing is currently well within pre-launch specifications, engineering tests with ISOCAM are ongoing in order to see whether the pointing can further be improved.

6. Discussion

In the previous sections we have described the basic approach for producing spectrophotometry with SWS, and provided instrumental uncertainties by systematic comparison of observed to reference continuum levels of the ACSs. The uncertainties may be dominated by ISO's pointing performance (Sec. 5), in-orbit characterization of the RSRF (Sec. 4), or the nature of the ACSs and input reference SEDs (Sec. 3). However, several instrumental and data processing effects such as reproducibility, detector memory and hysteresis effects, and, even more importantly, dark current subraction contribute to total continuum error budget of Table 1.

Proper dark current subtraction can be difficult where cosmic particle events have distorted the shape of the signal ramps over a number of reset intervals. Unrealistic (e.g., negative) flux levels may result at longer wavelengths (Band 4) when the source signal is less than a few Jy and changes in the dark current and "glitched" data are not well characterized. At *any* flux level, poor dark subtraction followed by flat-fielding will leave residual features of the RSRF in the final spectrum.

For flux densities below $\sim$1000 Jy hysteresis effects of all detectors can be neglected. Higher signals affect detector Bands 2 and 4 in the upscan, immediately following dark current measurement within an AOT. The deviation of the upscan from the downscan can be up to 20% depending on the signal, but decreases with typical time constants of 20-30 seconds. No hysteresis effects related to the grating scanner mechanisms have been observed.

In order to evaluate the reproducibility of the grating sections, a specific AOT2 observation of γ Dra was repeated twelve times (eight in the same revolution) using the same guide star. The comparison of the results shows that the derived fluxes vary (peak-to-peak) by 6% for detector Band 1, 12% for Band 2, 13% for Band 3, and 15% for Band 4. The pointing of ISO and dark current subtraction in the data processing are the main contributors to these dispersions. Further experiments are underway to verify reproducibility of different AOTs executed consecutively on the same source.

Fringing at different amplitudes and frequencies over Bands 1, 2, and 3 will impact line profiles and flux values. The extent of the fringing depends on the specific AOT observing mode, detector block, spatial extent of the source, and whether or not the line is resolved or unresolved. A pointing error of a few arcseconds on an extended source may give a slight shift in the phase of the fringes with respect to the calibration tables, translating to a *potential* uncertainty of $\sim$25% in the flux of an unresolved line in Band 3A, where the fringe amplitude is highest. Interactive Fourier techniques are successful in removing much of the fringing, but low instrumental sampling in fast AOT1 scans is not particularly accommodating to Fourier analysis without artificial resampling. Resolved lines in both point and extended sources are less susceptible to the fringing, and thus carry the same photometric uncertainties as the continuum fluxes.

While the current photometric uncertainty of SWS at all wavelengths is, in *most* cases, equal to or better than the desired pre-launch specification of 30%, the above data processing issues together with the impacts of the in-orbit relative responsivities and satellite pointing are focal points in our efforts for further improvement.

Acknowledgements. The authors wish to thank the GBPP consortium and members of the Calibration Working Group for laying the groundwork of ISO's calibration, including Drs. P.L. Hammersley and T. Müller for their contributions and helpful discussions. The contributions of Drs. R.A. Bell, B. Gustafsson, and K. Eriksson are also appreciated. The SWS Instrument Dedicated Team thanks the Vilspa support staff for their work, made successful by tolerating ours.

References

Bell R.A., & Gustafsson B. 1989, MNRAS 236, 653
Cohen, M., Walker, R.G., & Witteborn, F.C. 1992a, AJ 104, 2030
Cohen, M., Walker, R.G., Barlow, M.J., & Deacon, J.R. 1992b, AJ 104, 1650
Cohen, M., Witteborn, F.C., Walker, R.G., Bregman, J., & Wooden, D.H. 1995, AJ 110, 275
Cohen, M., Witteborn, F.C., Carbon, D.F., Davies, J.K., Wooden, D.H., & Bregman, J.D. 1996, AJ, in press
de Graauw, Th., Haser, L.N., Beintema, D.A., et al. 1996, A&A, this issue
Gustafsson B., Bell R.A., Eriksson K., & Nordlund Å. 1975, A&A 42, 407
Kurucz, R.L. 1992, Rev. Mex. Astron. Astrofis., 23, 181.
van der Bliek, N. S., Bouchet, P., Habing, H., et al. 1992, Msngr, 70, 28
van der Bliek, N. S., Gustafsson, B., & Eriksson, K. 1996a, A&A, 309, 849
van der Bliek, N. S., Waters, L. B. F. M., Bell, R.A., et al. 1996b, A&A, in review
Valentijn, E.A., Feuchtgruber, H., Kester, D.J.M., et al. 1996, A&A, this issue